A98-31702 ICAS-98-7,4,4

NON-REFLECTING BOUNDARY CONDITIONS FOR NON-LINEAR EULER CALCULATIONS USING AN IMPLICIT APPROACH

Olga V. Tchernycheva*
Royal Institute of Technology
Chair of Heat and Power Technology
S -100 44 Stockholm, Sweden

In numerical calculations of the flow through turbomachinery blade rows, it is often essential to introduce artificial boundaries to limit the area of computation. These artificial boundaries and boundary conditions must affect the solution in a manner such that it closely approximates the free space solution which exists without these boundaries. In practical, it means that the amplitudes of waves reflected from these artificial boundaries have to be minimized and hopefully eliminated. In concept, they correspond to the non-reflecting boundary conditions used in time-linearized methods.
Accurately predicting the behavior of complex unsteady flows with explicit computational analysis can require enormous computer resources. In order to decrease it and make the solver feasible for single processor use different methods are used. Implicit numerical analysis and dual time step marching are some of them.
In the present paper, numerical solutions are presented for two-dimensional Eulerian gasdynamic equations using an implicit approach for the flow field and for the boundary conditions. For the field a first order implicit scheme of Beam-Warming type on a second order Van Leer flux vector splitting is used. The boundary conditions are based on the characteristic form of the linearized Euler equations. With selected test cases, the importance of a correct simulation of the boundary conditions for stability margin of the blade rows is clearly demonstrated. It is shown that the result of numerical flow calculations is depend more on quality of boundary conditions, and less on the size of computational domain.

Introduction

Modern trends in turbomachinery design involve more loaded and longer blades, and new, often less forgiving, materials. It is thus that aeroelastic problem of High Cycle Fatigue (HCF) character will become of larger importance in the future.
A lot of research on High Cycle Fatigue in turbomachines has been performed with time-linearized flow solvers. It has been known for many years that the correct simulation of the inlet and outlet boundary conditions for cascades is important to establish the flutter boundaries for specific blade geometry and operating conditions. The inlet and outlet boundary conditions have to be "non-reflecting" in the sense that a far-field analytic small perturbation solution has been matched to the field solver to let all perturbations move out of the computational domain in a non-attenuated way.
With assumption that the waves are parallel to the boundary, with uniform pressure and prescribed total enthalpy and/or velocity, the approximate two-dimensional inlet and outlet conditions have been developed[1,2,3]. Certain limits towards application of inlet/outlet boundary conditions exit. But recently it has been shown[4] that a time-accurate explicit method can, with the proper formulation of the boundary conditions as two-dimensional highly non-reflecting, give results that agree with the small perturbation models also close to the acoustic resonance.

Physical model and mathematical description

The physical model in this study considers time-dependent flow, with negligible body forces, of a perfect gas through a two-dimensional cascade (compressor or turbine) (Fig.1).

* Graduate Student

Tchernycheva

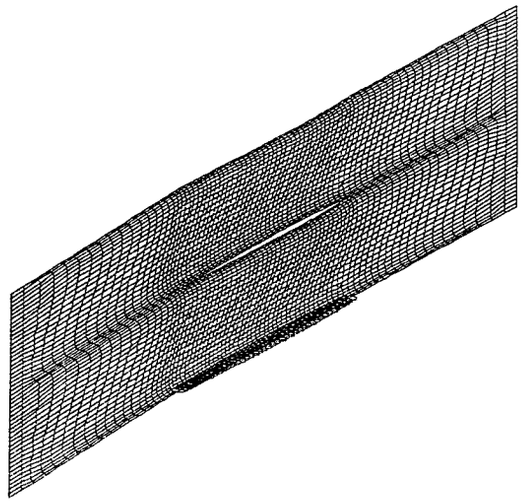

FIGURE 1 - General blade cascade

The unsteadiness in the flow is assumed to be caused by blade vibrations. The form of these vibrations are prescribed by function of space co-ordinates, (x, y), and time t.

To describe the flow around the vibrating cascade the time-dependent Euler two-dimensional equations are considered. The strong conservation-law form of these equations in a curvilinear boundary-fitted coordinate, (ξ, η), along the axial circumferential direction respectively, is given as follows

$$\partial_t \hat{Q} + \partial_\xi \hat{F} + \partial_\eta \hat{G} = 0$$

where $\hat{Q}$ is the vector of conservative variables, $\hat{F}$ and $\hat{G}$ are the inviscid flux vectors

$$\hat{Q} = Q/J$$
$$\hat{F} = (\xi_t Q + \xi_x F + \xi_y G)/J$$
$$\hat{G} = (\eta_t Q + \eta_x F + \eta_y G)/J .$$

The Jacobian of the transformation from physical (x, y) to computational (ξ, η) co-ordinates is

$$J = x_\xi y_\eta - y_\xi x_\eta$$

and the metric terms are

$$\xi_x = y_\eta/J \qquad \xi_y = -x_\eta/J$$
$$\eta_x = -y_\xi/J \qquad \eta_y = x_\xi/J .$$

In the Cartesian co-ordinate system, the conserved variables and inviscid flux vectors are

$$Q = (\rho, \rho u, \rho v, e)^T$$
$$F = (\rho u, \rho u^2 + p, \rho uv, (e + p)u)^T$$
$$G = (\rho v, \rho uv, \rho v^2 + p, (e + p)v)^T$$

The pressure p is related to density ρ and total energy e through the equation of state for an ideal gas, $p = (\gamma - 1)\left[e - \rho(u^2 + v^2)/2\right]$.

Solution Algorithm

An implicit unsteady Euler solver with first order accurate upwind biased second order flux difference splitting scheme is employed. The inviscid fluxes are discretized according to the Van Leer flux-vector splitting[5]. An alternative direction, approximate-factorization technique based in the Beam-Warming scheme[6] is used to compute the time rate changes in conservative variables.

Mesh movement

The mesh of the computational domain is body fitted such that mesh lines follow the actual boundaries (Fig.1). The mesh is of H-type with inlet and exit at the constant axial co-ordinates. As the blades vibrate, the computational grid must be modified to follow the blade motion. In the present study the mesh at one instant of time is computed by applying deflections to the nodes of the steady state mesh. These deflections are obtained through sine function interpolation along the grid lines of the deflections at the upper and lower boundaries. This method is fast and works well for small amplitudes of any type of motion. For larger amplitudes, however there is a risk of getting inverted cells and some other method should then be used.

Boundary conditions

The inlet and exit boundary conditions used in this study are based on a characteristic analysis of the linearized Euler equations. In the present analysis, quasi-two-dimensional characteristic boundary conditions are solved implicitly along with inlet and outlet part of the computational domain[7].

The standard procedure is used to establish the non-penetration conditions. It gives for the unsteady case a flux-vector on the wall, which is completely determined if the wall pressure is known.

The periodic boundary is implemented with a direct store method[8].

Tchernychova

Inlet and Exit Boundary Conditions

These boundary conditions are in the present analysis solved as a part of the implicit solution procedure. The algorithm for the boundary condition has been proposed by Chakravarthy[7] and can be regarded as a two-dimensional approximation. Consider an approximate factorization scheme, written in semi-discretized form as

$$\left[I + \Delta t J^{n+1}\left(\partial_\xi \hat{A}^n\right)\right]\left[I + \Delta t J^{n+1}\left(\partial_\eta \hat{B}^n\right)\right]\Delta Q =$$
$$= -\left(1 - J^{n+1}/J^n\right)Q^n - \Delta t J^{n+1}\left(\partial_\xi \hat{F} + \partial_\eta \hat{G}\right)^n \tag{1}$$

where $\hat{A} = \frac{\partial \hat{F}}{\partial Q}$, $\hat{B} = \frac{\partial \hat{G}}{\partial Q}$ are Jacobians matrices.

Defining the right handside part of equation (1) by $\overline{\Delta Q^n}$ and $\left[I + \Delta t J^{n+1}\left(\partial_\xi \hat{A}^n\right)\right]\Delta Q^n$ by $\overline{\overline{\Delta Q^n}}$, the solution in time is given by solving the two coupled tridiagonal systems

$$\left[I + \Delta t J^{n+1}\left(\partial_\eta \hat{B}^n\right)\right]\overline{\Delta Q^n} = \overline{\Delta Q^n} \tag{2}$$

$$\left[I + \Delta t J^{n+1}\left(\partial_\xi \hat{A}^n\right)\right]\Delta Q = \overline{\overline{\Delta Q^n}} \tag{3}$$

The boundary conditions are applied to the equation (3) under assumption that only the waves transported normal to the boundary (in our case this boundary is a $\xi = const.$ surface) are considered. First, the equation (3) is transformed to characteristic form by multiplying by the left eigenvectors, T_ξ^{-1}, of the $\hat{A}$ matrix

$$T_\xi^{-1}\left[I + \Delta t J^{n+1}\left(\partial_\xi \hat{A}^n\right)\right]\Delta Q = T_\xi^{-1}\overline{\overline{\Delta Q^n}} \tag{4}$$

The equation (4) is the starting point to apply the desired boundary conditions. Outgoing waves, which are propagating from the inner computational domain towards the boundary are completely determined by the interior field solution. For these waves the equation (4) remains unchanged. Incoming waves, on the contrary, are to be replaced by non-reflecting boundary conditions. It means that all incoming waves are suppressed which is expressed by vanishing time derivative of the corresponding characteristic variables of the $\hat{A}$ matrix. Finally, the equation (4) with non-reflecting conception of boundary conditions looks like

$$\left[T_\xi^{-1} + \Delta t J^{n+1} L T_\xi^{-1}\left(\partial_\xi \hat{A}^n\right)\right]\Delta Q = T_\xi^{-1}\overline{\overline{\Delta Q^n}}$$

where L matrix is depended on the flow situation at the boundary (subsonic or supersonic) and on which boundary it is applied (inlet or outlet). So, there are following possibilities to define the L matrix:
- for subsonic case

at the inlet

$$L = \begin{pmatrix} 0 & 0 & 0 & 0 \\ 0 & 0 & 0 & 0 \\ 0 & 0 & 0 & 0 \\ 0 & 0 & 0 & 1 \end{pmatrix}$$

at the outlet

$$L = \begin{pmatrix} 1 & 0 & 0 & 0 \\ 0 & 1 & 0 & 0 \\ 0 & 0 & 1 & 0 \\ 0 & 0 & 0 & 0 \end{pmatrix}$$

- for the supersonic case

at the inlet $L = 0$

at the outlet $L = I$

The implicit boundary conditions outlined above are made for waves that approach the boundary at normal incident and represent approximate, quasi-two-dimensional, nonreflecting boundary conditions which can be used for steady and unsteady flow simulations.

Surface Boundary Conditions

For the moving blades the non-penetration or kinematic boundary condition, for inviscid flow, requires that the velocity component of the flow normal to the blade surface must equal to the velocity component of the blade normal to the blade surface

$$\vec{u} \cdot \vec{n} = \vec{u}_{blade} \cdot \vec{n}$$

where $\vec{n}$ is the normal to the blade surface.
The generalised $\hat{G}$-flux at the wall becomes

$$\hat{G} = \begin{pmatrix} 0 \\ \eta_x p \\ \eta_y p \\ -\eta_t p \end{pmatrix}$$

The pressure is obtained by extrapolation (in transformed space) from the interior of the field to the boundary along a grid line. The velocity component parallel to the blade is set through zero-order extrapolation from the closest interior cell and density and energy are set by linear extrapolation.

Periodic Boundary Condition

Periodic boundary condition is applied in the blade-to-blade direction. The calculations are carried out in an area just containing a single blade passage but by this periodic condition they are simulating a cascade containing an infinite number of blade.
The standard treatment is to make the boundary as a part of the field by adding ghost cells outside the boundary. For steady flow, the values in the ghost cells along the upper boundary are copied from the values in the cells at the bottom of the computational domain and vice versa at the lower boundary

$$Q_{UG} = Q_{LI}$$
$$Q_{LG} = Q_{UI}$$

where UG refers to "upper ghost" and LI refers to "lower ghost". However, for unsteady flow, if the blade have the phase difference, ϕ, in their motion the values in the ghost cells must be phase lagged accordingly

$$Q_{UG}(\omega t) = Q_{LI}(\omega t - (2\pi - \phi))$$
$$Q_{LG}(\omega t) = Q_{UI}(\omega t - \phi)$$

Applying the so called direct store method[4] requires that the time history of the flow for at least one cycle is saved. In the present method, under relaxation is applied to the periodic boundary to improve stability.

Results and discussion

To show the general performance of the present method comparisons have been made with other numerical prediction methods. The codes used for comparison are LINSUB[1] and INST[4]. LINSUB is potential flow solver for calculating the subsonic flow around flat plates. It is based on a linear singularity theory. INST is a two-dimensional non-linear Euler solver for flow through vibrating blade cascade. The flow algorithm employed in this code is based on Van Leer vector splitting[5] and on explicit predictor corrector type integration. There are several kinds of boundary conditions, which are implemented in this code: steady, Giles one- and two-dimensional[3] and highly non-reflecting[4]. The last one uses the Fourier decomposition in both time and space and are truly non-reflecting for all waves. More details on these boundary conditions can be found in [4].
For the unsteady results the first harmonic of the dimensionless pressure $\tilde{C}p$ is presented

$$Cp(x,y,t) = \overline{C}p(x,y) + \tilde{C}p(x,y)e^{-i\omega t}$$

The pressure is non-dimensionalized using the difference between total and static pressures at the inlet and has been scaled linearly for torsion to the amplitude of one radian and for the bending to the amplitude of one chord length. Since $\tilde{C}p$ is a complex variable, it can be represented either as phase and magnitude (real amplitude) or as imaginary and real parts. Here, to plot the unsteady pressure along chord, the last representation will be used. For the flat plate cases, the plot over chord rather shows the unsteady pressure difference, $\Delta\tilde{C}p$, of lower and upper surfaces.

For each boundary conditions, the calculations were done for the short and long axially truncated domain with otherwise identical data. For the short domain, calculations with inflow and outflow ducts extended one axial chord length up- and downstream of the cascade, while for the long domain calculations the length of outflow was doubled (Fig.3).
Thus, the difference in the solutions for short and long domains can be consider as a measure of the reflectiveness of a particular boundary condition. And also the length of propagating waves, λ, must be taken into account, otherwise if the boundary conditions are not good enough, the result of the calculation will be the same on each domain extended wave length (Fig.2, point AA) in axial direction from an initial one (Fig.2, point A).

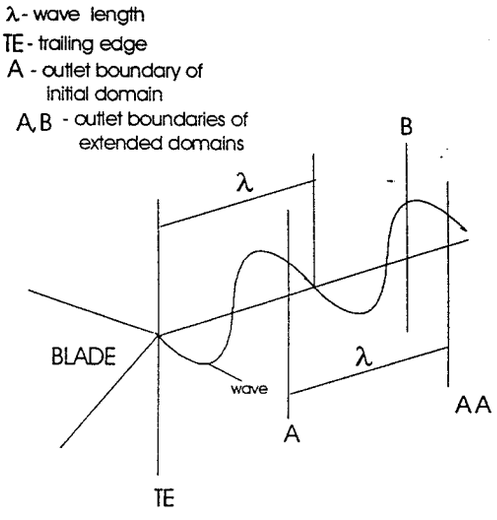

FIGURE 2 - Wave propagation

If the initial domain is extended to another value (Fig.2, point B) it is difficult apriori to say anything about the quality of the solution on this domain - it could be better or worse with the same probability. If the boundary conditions are correct this kind of problem does not appear.

All calculations have been made with small vibration amplitudes in order to be compared with numerical data, which are given by linearized solver LINSUB.

Flat-plate cascade

With comparison to cases with steady loading, where a considerable part of the unsteady loading can be result from the motion of the blades through a spatially non-uniform steady pressure field, for a flat-plate cascade all of the unsteady loading is directly affected by far-field boundary conditions.
The calculations have been made on the cascade with a pitch-to-chord ratio of one, stagger angle of 45 degrees and a uniform steady mean flow with Mach number of 0.7. The cascade performed torsional vibrations around mid-chord with amplitude of 0.5 at reduced frequency of 1.0, based on full chord and inlet velocity.
Results are shown for interblade phase angles, σ, of 0 and 90 degrees. Comparisons have been done for unsteady pressure difference distributions and aerodynamic moment coefficients.
Fig.3 and 4 shows the unsteady pressure contours for $\sigma = 0°$ and $\sigma = 90°$, respectively. As can be seen from these plots, for the blades vibrating in-phase (Fig.3) there are no significant waves in its downstream far-field, while for the blade vibrating out-of-phase (Fig.4) very strong waves are existent. So, for the second case correct far-field non-reflecting boundary conditions are demanding, because the pressure waves could be reflected by poor boundary conditions and the calculated pressure distribution along the blades would be far from the real physical one.

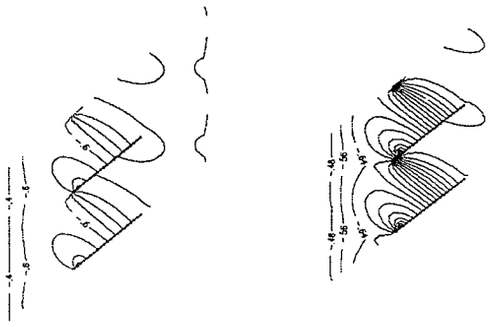

(A) Chakravarthy's 2D (B) Highly Non-Refl.

FIGURE3 - Unsteady pressure contours ($\sigma = 0°$) for the short domain.

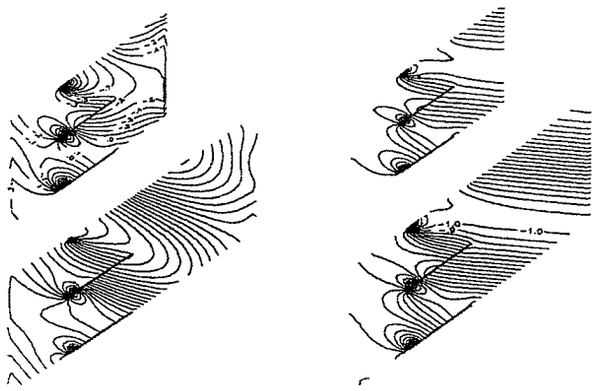

(A) Chakravarthy's 2D (B) Highly Non-Refl.

FIGURE 4 - Unsteady pressure contours ($\sigma = 90°$) for the short and long domains.

For flutter analysis the aerodynamic damping, Ξ_α, is an important characteristic. For torsional vibrations it is given by the negative imaginary part of the moment coefficient.
Fig.5 shows the aerodynamic damping over interblade phase angle for the short domain.

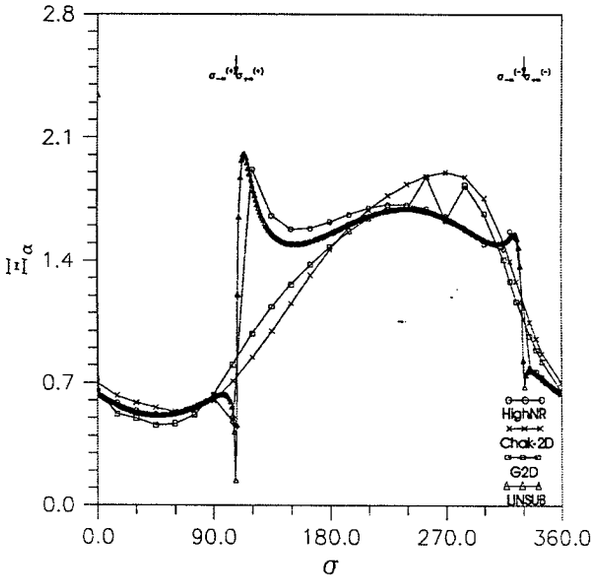

FIGURE 5 - Aerodynamic damping (short domain)

As can be seen the comparison between LINSUB and the highly non-reflecting boundary conditions is also good close to the resonance angles, at which the pressure waves are perfectly perpendicular to the boundary. The agreement with other boundary conditions is poor and this especially around the resonances.
Table 1 shows the aerodynamic damping for the short and long domains with $\sigma = 0°$.

Type of boundary conditions	Short domain	Long domain
Highly non-reflecting	0.6509	0.6509
Giles 2-dimensional	0.6514	0.6516
Chakravarthy' 2-dimensional	0.7021	0.6717
LINSUB	0.6387	

TABLE 1 - Damping of flat-plate cascade due to torsional vibrations ($\sigma = 0°$)

The results for all boundaries are quit close and do not depend on the size of computational domain. In this case vibrating blades do not generate any significant waves in its downstream far-field (Fig.3) and it can explain the quit good agreement for damping. From the unsteady pressure contours (Fig.3(A)) it becomes clear, why approximately two-dimensional nonreflecting boundary conditions produce good results. Upstream far-field shows waves, which are normal to the axial direction and these Chakravarthy's and Giles boundary conditions were made to capture such kind of waves.
For the 90 degrees interblade phase angle not all boundary conditions produce equally good results. Table 2 shows that only the highly non-reflecting boundary conditions give good agreement for damping coefficient for the short and long domains.

Type of boundary conditions	Short domain	Long domain
Highly non-reflecting	0.6123	0.6139
Giles 2-dimensional	0.6325	0.7374
Chakravarthy' 2-dimensional	0.5974	0.8407
LINSUB	0.6172	

TABLE 2 - Damping of flat-plate cascade due to torsional vibrations ($\sigma = 90°$)

However, the results for other boundary conditions, although they are both so-called approximately two-dimensional, are different for different size of domain. Reason for this is non-zero interblade phase angle, which impose a periodicity over the blade passages. It affect the wave pattern in the far-field as to require not only axially propagating waves (Fig.4). And highly non-reflecting boundary conditions can capture all kind of incoming waves, but other boundaries are able to consider only axially propagating ones. Moreover, for different size of domain the results can be better or worse and it is not apriori clear, that the result will improve with extension of the flow domain.
Fig.6 shows the pressure difference distributions with $\sigma = 0°$ for the short domain.

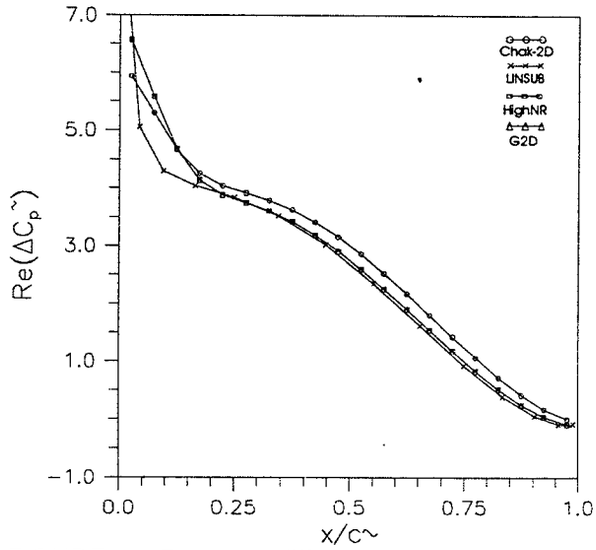

FIGURE 6 - Pressure difference distribution of flat-plate case due to torsional vibrations ($\sigma = 0°$) for the sort domain.

These distributions are quit close to each other and such confirm the good agreement of the damping data at $\sigma = 0°$. The pressure difference distributions for the long domain are not shown because they are practically indistinguishable from the results for the short domain. For $\sigma = 90°$ it is interesting to note that although all short domain calculations give about the right damping, the pressure difference distributions (Fig.7) and the unsteady pressure contours (Fig.4) for the approximate two-dimensional boundary conditions are quit different for the short and for the long domains.

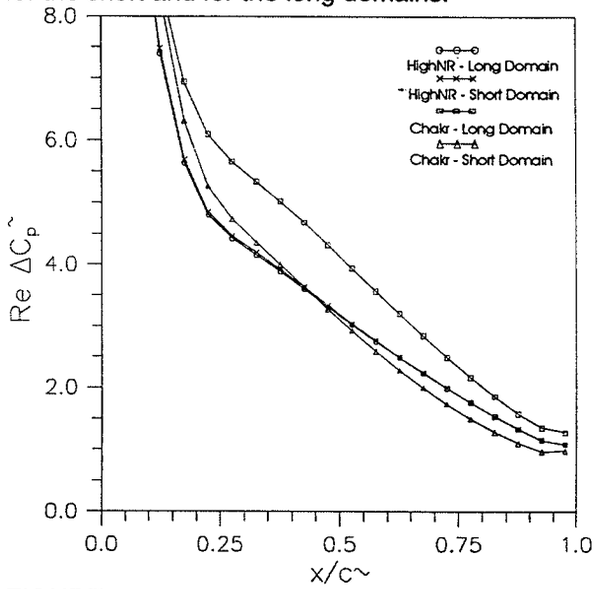

FIGURE 7 - Pressure difference distribution of flat-plate case due to torsional vibrations ($\sigma = 90°$)

The results for Giles boundary conditions are not shown because they are quit similar to the result for

Chakravarthy's ones. It is clear to see that the pressure difference distributions for Chakravarthy's boundary conditions has poor agreement with the result for the highly non-reflecting boundary conditions, which can be consider as exact solution[6].
Unfortunately it is not clear apriori where approximate boundary conditions will be sufficient and it depends more on the angle at which the waves cross the boundary. If pressure waves go almost parallel to the boundary then approximate two-dimensional boundary conditions produce reasonable pressure distribution along the blade. But it is evident that these boundary conditions cannot properly handle waves which are perpendicular to the boundary.

Compressor cascade

Here the cascade has a comparatively light steady loading. The blades of this cascade are 2.7 percent thick, symmetric, sharp-edged airfoils with maximum thickness at mid-chord. The stagger angle of the cascade is 59.3° and the pitch-to-chord ratio is 0.95. This cascade is the Fifth Standard Configuration from a series of aeroelastic test cases[9].
With steady flow for Mach number of 0.5 and an incident angle of 2 degrees, the unsteady calculations have been done for torsional vibrations about mid-chord with amplitude 0.1 at a reduced frequency of 2.04.
Here the result by LINSUB for the flat-plate cascade with the same flow geometry as for the compressor cascade but with zero incidence angle ($i = 0°$) are presented as reference.
Table 3 shows the same behavior of damping data for different domain sizes as the second of the flat-plate cases.

Type of boundary conditions	Short domain	Long domain
Highly non-reflecting	0.9071	0.9174
Giles 2-dimensional	0.6301	0.9015
Chakravarthy' 2-dimensional	0.6579	0.8603
LINSUB ($i = 0°$)	0.9723	

TABLE 3 - Damping of compressor cascade due to torsional vibrations ($\sigma = 90°$)

But now the long domain results of two-dimensional Giles and Chakravarthy's conditions are in good agreement with highly non-reflecting ones, which can be consider again as correct solution. Fig.8 shows the pressure difference distribution, which is quit close for different boundary conditions.

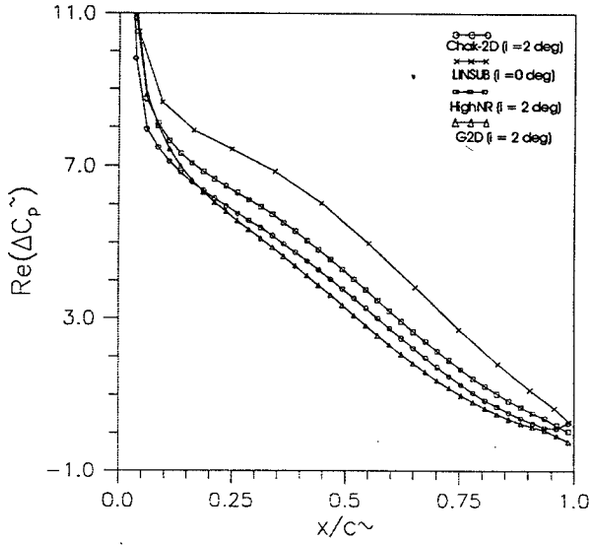

FIGURE 8 - Pressure difference distribution of compressor case due to torsional vibrations ($\sigma = 90°$) for the short domain.

Also the pressure difference distribution has quit reasonable agreement with one reproduced by LINSUB. Fig.8 shows also that for preliminary description of flow behavior around compressor blades at low incidence the flat-plate model can be used, because it gives good qualified agreement and takes less computational time.
But a right damping does not necessarily correspond to locally correct result. And the unsteady pressure distribution given by Fig.9 shows that neither of the two-dimensional Giles and Chakravarthy's results are accurate.

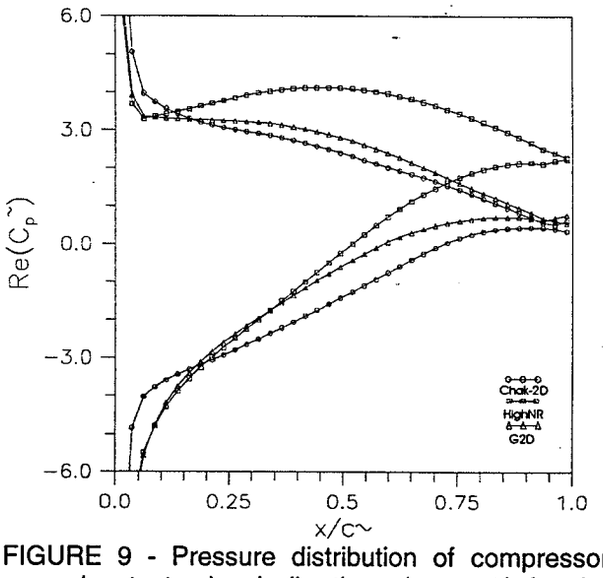

FIGURE 9 - Pressure distribution of compressor case due to torsional vibrations ($\sigma = 90°$) for the short domain.

The difference in the pressure distributions between the various boundary conditions is greater than the difference in the pressure difference distributions. It can be explained that the effect of poor boundary conditions is a shift of the pressure levels, while the pressure difference between low and upper blade surface is still more or less the same as for the correct boundary conditions.

Conclusions and Perspectives

Steady and unsteady boundary condition procedures for implicit turbomachinery analysis have been implemented in numerical way. Comparisons have been done with two-dimensional Giles and highly non-reflecting boundary conditions. It was shown that all boundary conditions give good results when the pressure waves propagate in a nearly normal direction to the boundary, while for the waves which are perpendicular to the boundary only highly non-reflecting boundary conditions are sufficient. But these boundary conditions are available only for explicit turbomachinery analysis. Thus, this article reminds one more time that highly non-reflecting implicit boundary conditions are necessary. They will allow to make a full implicit approach with correct inlet and outlet boundary conditions, that will able to decrease computational time significantly. This work is presently in progress.

Acknowledgment

The author would like to thank Prof. T.H.Fransson, Mr. A.Krainer, Mr. F.Moyroud, Mr. W.Höhn for helpful conservations during the preparation of the article.

References

[1]Smith, S.N., "Discrete Frequency Sound Generation in Axial Flow Turbomachines", PhD Dissertation, Cambrige University, Engineering Department, UK, 1971.

[2]Acton, E., Cargill, A. M., "Non-reflecting boundary conditions for Computations of Unsteady Flows in Turbomachines", Unsteady Aerodynamics and Aeroelasticity of Turbomachines and Propellers, edited by H.E.Gallus and S.Servaty, 1987, pp.221-228.

[3]Giles, M.B., "Non-reflecting Boundary Conditions for Euler Equation Calculations", AIAA Journal, Vol. 28, No.12, 1990, pp.2050-2058.

[4]Krainer, A.F., Hambræus, T., Fransson, T.H., "Highly Non-reflecting Boundary Conditions for Non-linear Euler Calculations of Unsteady Turbomachinery Flows", submitted to AIAA Journal of Propulsion and Power, 1996.

[5]Van Leer, B., "Flux Vector Splitting for the Euler Equations", ICASE Report No. 82-30, 1982.

[6]Beam, A.; Warming, R.F., "An Implicit Finite-Difference Algorithm for Hyperbolic Systems in Conservation-Law Form", Journ. Comp. Phys., Vol. 22, 1976, pp. 87-110.

[7]Chakravarthy, S.R., "Euler Equations - Implicit Schemes and Boundary Conditions", AIAA Paper 82-0228.

[8]Siden, L.D.G., "Numerical Simulation of Unsteady Viscous Compressible Flows Applied to Blade Flutter Analysis", ASME Paper 91-GT-203, 1991.

[9]Bölcs, A., Fransson, T.H., "Aeroelasticity in Turbomachines Comparison of Theoretical and Experimental Cascade Results", Air Force Office of Scientific research, AFOSR-TR-87-0605, 1986.